Electronic Supplementary Information

Acoustic Focusing With Engineered Node Locations for High-Performance Microfluidic Particle Separation

Erika J. Fong,[a,b] Amanda C. Johnston,[a] Timothy Notton,[c] Seung-Yong Jung,[c] Klint A. Rose,[a] Leor S. Weinberger[c] and Maxim Shusteff*[a]

[a] *Lawrence Livermore National Laboratory, 7000 East Ave., Livermore, CA, 94550 USA. Fax: +1-925-422-2783; Tel: +1-925-423-0733; E-mail: shusteff1@llnl.gov*
[b] *Department of Biomedical Engineering, Boston University, 44 Cummington St., Boston, MA, 02215 USA*
[c] *The Gladstone Institutes, Department of Virology and Immunology, University of California, San Francisco, CA 94158, USA*

S1 Focusing Performance in GEN1 Devices

Figure S1 summarizes the results of *in situ* focusing measurements (as described in the main article "Materials and Methods: *In situ* calibration" section) from 18 distinct GEN1 devices, spanning 11 different design configurations, with walls of different locations and thicknesses t_W. As expected, the resonant frequency f_0 increases with increasing t_W. This is because the wall reduces the effective "water equivalent" channel width w_{eff} due to the six-fold faster speed of sound in silicon relative to water. This effective width is estimated as $w_{\mathrm{eff}} = w_T - t_W(1 - c_w/c_{\mathrm{Si}})$ where c_w and c_{Si} are the speed of sound in water and silicon, respectively. Resonant frequencies are then calculated as $f_0 = nc_w/2w_{\mathrm{eff}}$, where n is the number of pressure nodes (2 for our device). The expected values f_0 are shown in Fig. S1(a) with a dashed line, calculated for temperatures of 30 °C and 40 °C. The average f_0 measured in 1mm chips with no wall is 1.49 MHz, and experimentally measured values generally match predicted values better for thinner walls. This first-order analysis is certainly an incomplete model of resonance within the full 3-dimensional physical system, and underestimates f_0 for thicker wall widths, but provides useful estimates when the wall is thin (Fig. S1(a)).

Fig. S1(b) shows pressure node locations, measured from the nearest channel wall, along with calculated locations based on the values of w_{eff}. As with the peak frequency data, thinner walls are in closer agreement with calculations, and with less overall scatter in the measured data. Finally, as expected, Fig. S1(c) confirms that increasing the wall thickness beyond 30 µm has a negative impact on focusing efficiency, in some cases severely. The notable exceptions to this general trend are the devices with 750 µm separation channels and 80 µm and 40 µm walls (referred to as "750-80" and "750-40" devices). These perform very well, relative to their w_{SEP} = 650 µm counterparts, though not quite as well as thinner wall chips. The probable reason for this, as well as for the relatively large overall scatter in the data for GEN1 devices is the quality and thickness of the adhesive layer between the piezo actuator and the silicon. This parameter of device assembly was not tightly controlled in GEN1 devices compared with GEN2 devices. The 750-80 and 750-40 chips likely had exceptional acoustic coupling properties relative to the other GEN1 chips. We similarly attribute the substantial differences in peak frequency and node position for the w_T = 32 µm devices to piezo attachment variations.

Prior to assembly of GEN2 devices, we developed a procedure for dispensing a controlled volume of low-viscosity cyanoacrylate without introducing voids or thickness non-uniformity. A direct performance comparison between identical devices before and after the improved adhesive procedure is showin in Fig. S2. Furthermore, the improved coupling of the piezo transducers to the acoustic chips in GEN2 devices, resulting in more consistent delivery of acoustic power to the channel, is apparent from the significantly tighter error bars for both the focusing location and FWHM data, even at lower voltages and higher flow speeds than those used to characterize GEN1 devices (Fig. S3).

In spite of the variability in these trends, the data in the aggregate points toward thinner walls allowing higher-efficiency focusing with less dependence on wall position. Minimizing wall thickness t_W ensures that the focusing position can be designed without regard to the wall, and the wall's effects on operating frequency and separation efficiency can be neglected. For this reason, all GEN2 devices were designed with 16 µm walls, which is the thinnest that can be reliably fabricated.

S2 DENV2 PCR Quantitation Protocol

Dengue virus quantitation at the chip outlets relative to the input sample was accomplished by amplifying an 80-base-pair sequence by quantitative reverse-transcription polymerase chain reaction (qRT-PCR), with primer sequences 5'-CATATTGACGCTGGGAAAGAC-3' (forward) and 5'-TTCCATTTTCTGGCGTTCTGTG-3' (reverse). Amplification was monitored with a fluorescently-labelled reporter probe (5'-AGATCCTGCTGTCTCCTCAG-3'). Each amplification reaction contained 5 µL of sample and 20 µL of master mix, based on SuperScript III enzyme chemistry (Invitrogen). Thermal cycling was initiated with a 30 minute hold at 48 ° C for reverse transcription, then a 15-minute hold at 95 °C, followed by 40 cycles of 20 s at 94 °C to denature, 10 s at 55 °C to anneal, and 30 s at 72 °C to extend. The primer and probe sequences have been tested in silico against all known sequences in NIH GenBank, with no significant sequence similarity found. They have also been screened against over 58 prokaryotic and eukaryotic organisms, including human DNA, in addition to more than 2000 environmental samples, and 12 cell lines with no significant cross-reactivity observed.

S3 Video of Real-time Separation of 10 µm and 200 nm Fluorescent Beads

Separation of 10 µm (red) and 200 nm (green) fluorescent beads using a 3-pass, w_{SEP} =280 µm GEN2 device at $10V_{pp}$. Average linear flow velocity is 60 mm/s. Videos for the 10 µm beads were captured with a TRITC filter, and the 200 nm beads were captured with a FITC filter and the acoustic field was turned on and off manually at specified time points. The two videos were then merged. The video is in real time.

Figure S1 First-generation (GEN1) *in situ* characterization results plotting (a) peak frequency, (b) focusing location and (c) focusing efficiency for different wall widths t_W and separation channel widths w_{SEP}. Error bars represent one standard deviation for n=3 or greater. Dashed lines are calculations based on the speed of sound in silicon and water. In (a) the upper dashed line is calculated at 40 °C, and the lower line at 30 °C, while in (b) the difference between calculated peak locations at 30 and 40 °C was insignificant.

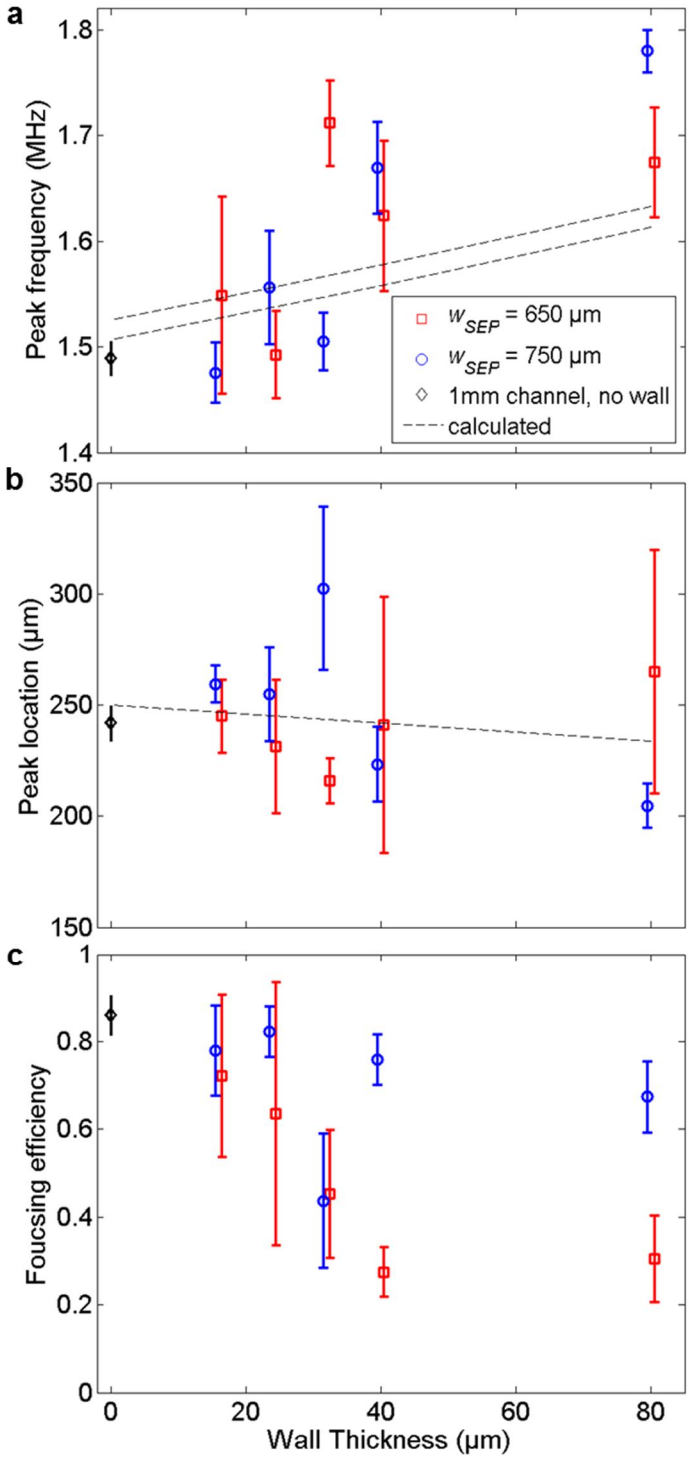

Figure S2 Characterization and comparison of a 3-pass, w_{SEP}=280 µm GEN2 device before (high viscosity) and after (low viscosity) optimizing the piezo transducer gluing procedure, showing (a) peak location and (b) focusing width. Average linear flow velocity for points shown in red was 60 mm/s and blue 20mm/s. (n=3)

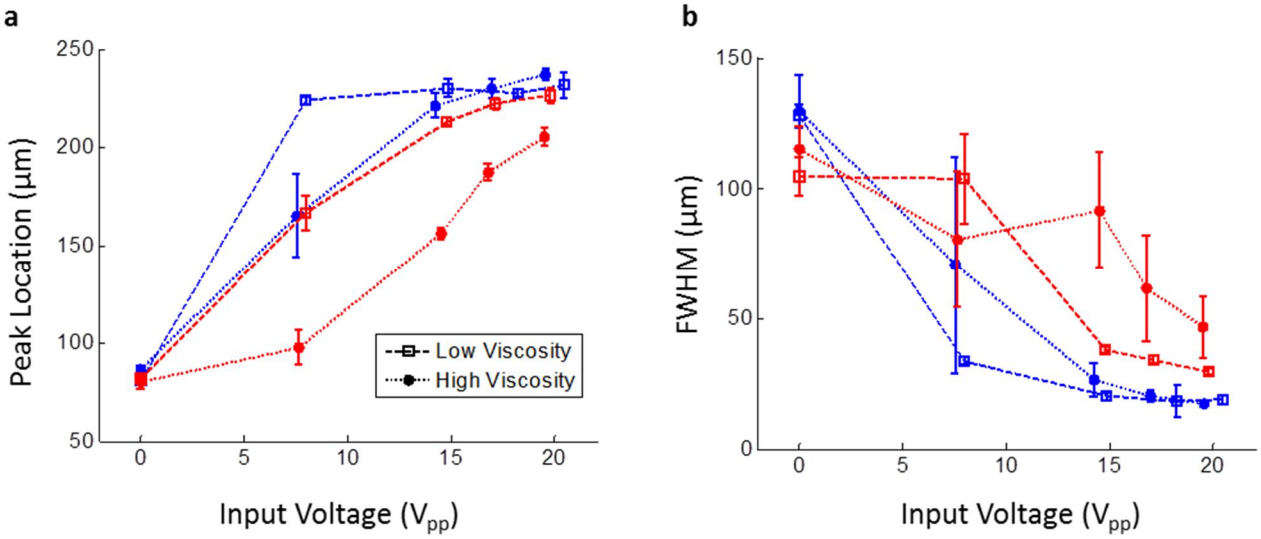

Figure S3 Characterization and comparison of 3-pass GEN2 devices with walls at different locations, w_{SEP}=280 and w_{SEP}=300 µm, showing (a) peak location and (b) focusing width. Average linear flow velocity is 20mm/s, n=4 or greater.

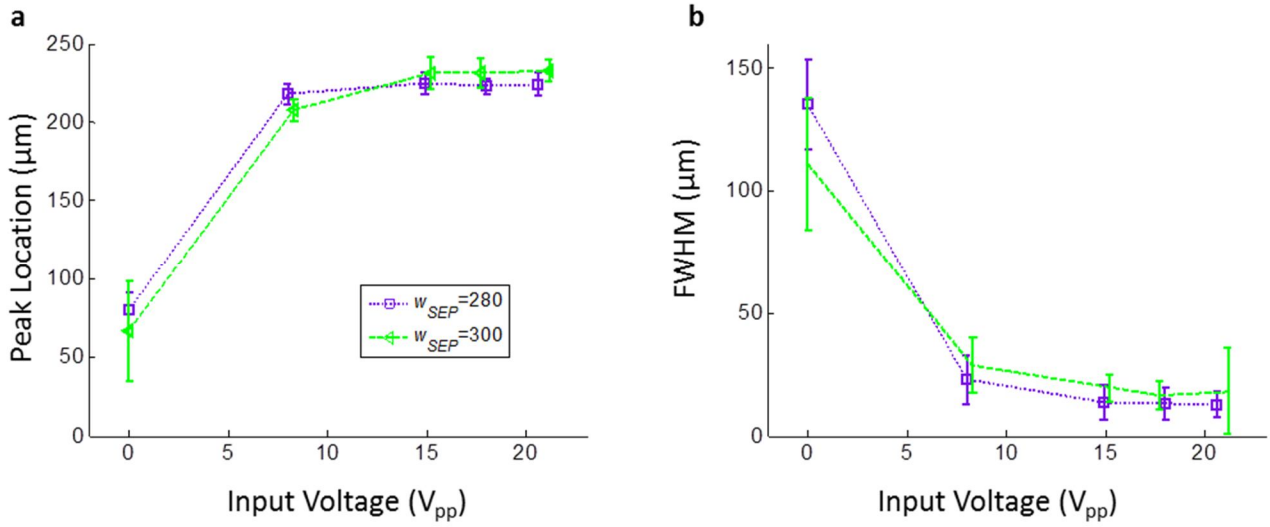

Figure S4 Recovery of polymer microspheres of different sizes in the LPO (clean buffer stream) at different operating voltages, using a 3-pass, w_{SEP} =300 µm GEN2 device, n=3. Average linear flow velocity is 60mm/s. This data serves as an approximate calibration curve to estimate the required driving voltages for extracting particles of a particular size. For example, at 15.2 V_{pp} the device is expected to extract approximately 90% of 8 µm particles and less than 5% of 1 µm particles.

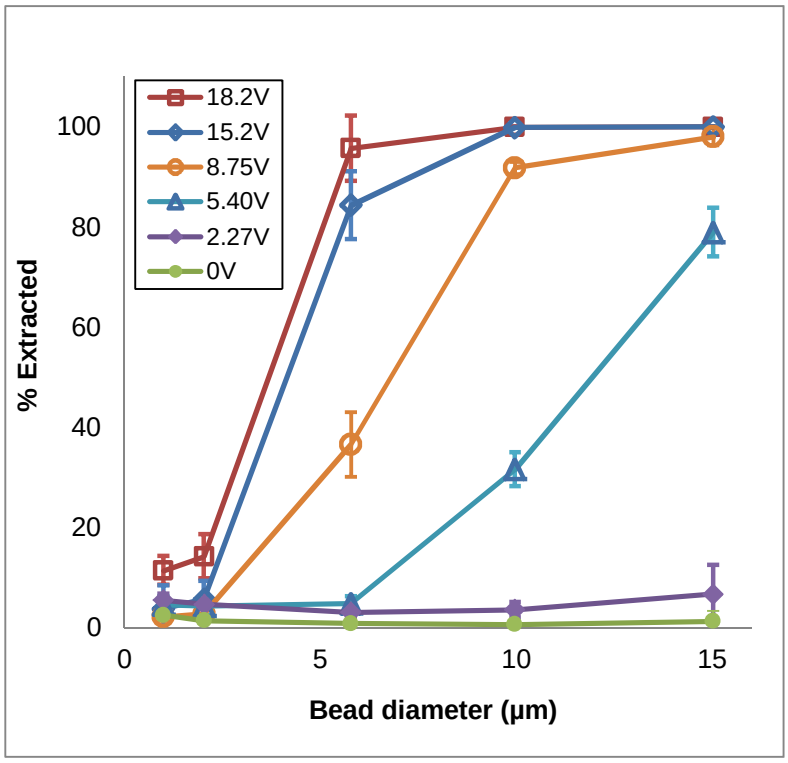

Figure S5 Fraction of Raji cells extracted in the large particle outlet (LPO) as a function of voltage supplied to the piezo transducer.